Surgical Oncology 28 (2019) 1–8

Contents lists available at ScienceDirect

Surgical Oncology

journal homepage: www.elsevier.com/locate/suronc

Fluorescence-guided tumor detection with a novel anti-EpCAM targeted antibody fragment: Preclinical validation

Leonora S.F. Boogerd[a,1], Martin C. Boonstra[a,1], Hendrica A.J.M. Prevoo[a], Henricus J.M. Handgraaf[a], Peter J.K. Kuppen[a], Cornelis J.H. van de Velde[a], Alexander Fish[b], Robert A. Cordfunke[c], A. Rob P.M. Valentijn[d], A.G. Terwisscha van Scheltinga[d], Glen C. MacDonald[e], Jeannick Cizeau[e], Arjune Premsukh[e], Maaike L. Vinkenburg van Slooten[a], Jacobus Burggraaf[f,g], Cornelis F.M. Sier[a,h], Alexander L. Vahrmeijer[a,*]

[a] Leiden University Medical Centre, Department of Surgery, Leiden, the Netherlands
[b] Netherlands Cancer Institute, Division of Biochemistry, Amsterdam, the Netherlands
[c] Leiden University Medical Centre, Department of Immunohematology and Blood Transfusion, Leiden, the Netherlands
[d] Leiden University Medical Centre, Department of Clinical Pharmacy and Toxicology, the Netherlands
[e] Viventia Biotechnologies Inc., Winnipeg, MB, Canada
[f] Centre for Human Drug Research, Leiden, the Netherlands
[g] Leiden Academic Center for Drug Research, Leiden, the Netherlands
[h] Antibodies for Research Applications BV, Gouda, the Netherlands

ARTICLE INFO

Keywords:
Epithelial cell adhesion molecule
Fluorescence
Surgery
NIR
Colorectal cancer
IRDye800CW

ABSTRACT

Tumor-specific fluorescent imaging agents are moving towards the clinic, supporting surgeons with real-time intraoperative feedback about tumor locations. The epithelial cell adhesion molecule (EpCAM) is considered as one of the most promising tumor-specific proteins due its high overexpression on epithelial-derived cancers. This study describes the development and evaluation of EpCAM-F800, a novel fluorescent anti-EpCAM antibody fragment, for intraoperative tumor imaging. Fab production, conjugation to the fluorophore IRDye 800CW, and binding capacities were determined and validated using HPLC, spectrophotometry and cell-based assays. *In vivo*, dose escalation-, blocking-, pharmacokinetic- and biodistribution studies (using both fluorescence and radioactivity) were performed, next to imaging of clinically relevant orthotopic xenografts for breast and colorectal cancer. EpCAM-F800 targets EpCAM with high specificity *in vitro*, which was validated using *in vivo* blocking experiments with a 10x higher dose of unlabeled Fab. The optimal dose range for fluorescence tumor detection in mice was 1–5 nmol (52–260 μg), which corresponds to a human equivalent dose of 0.2–0.8 mg/kg. Biodistribution showed high accumulation of EpCAM-F800 in tumors and metabolizing organs. Breast and colorectal tumors could clearly be visualized within 8 h post-injection and up to 96 h, while the agent already showed homogenous tumor distribution within 4 h. The blood half-life was 4.5 h. This study describes the development and evaluation of a novel EpCAM-targeting agent and the feasibility to visualize breast and colorectal tumors by fluorescence imaging during resections. EpCAM-F800 will be translated for clinical use, considering its abundance in a broad range of tumor types.

1. Introduction

Prognosis after cancer surgery mainly depends on the completeness of the surgical resection [1–4]. Accurate detection of tumor margins during surgery can be difficult due to the lack of visual distinction between tumor and normal or inflamed/fibrotic tissue. This can be problematic especially after neoadjuvant chemo- and/or radiotherapy (CRT), which is frequently used in rectal cancer patients [5]. Targeted fluorescence-guided surgery (FGS) is an intraoperative imaging technique that allows real-time tumor identification. FGS is based on (near-infrared, NIR) fluorescent dyes in combination with a dedicated imaging system and is already widely investigated for sentinel lymph node

* Corresponding author. Albinusdreef 2, 2300, RC Leiden, the Netherlands.
E-mail address: a.l.vahrmeijer@lumc.nl (A.L. Vahrmeijer).
[1] Both authors contributed equally and share first authorship.

https://doi.org/10.1016/j.suronc.2018.10.004
Received 5 February 2018; Received in revised form 13 September 2018; Accepted 8 October 2018

mapping, liver tumor detection and bile duct imaging using the non-targeted fluorescent dye indocyanine green [6]. Conjugating fluorescent dyes to specific tumor-recognizing ligands, such as antibodies or peptides, enhances the specificity of this technique for tumor imaging considerably. Various tumor-specific agents have already shown feasibility in early phase clinical trials [7–11].

Not all tumor-associated biomarkers are suitable targets for imaging purposes; prerequisite is expression on the cellular membrane with several fold higher densities compared to surrounding normal cells [12]. The Epithelial Cell Adhesion Molecule (EpCAM) was among the first human tumor-associated antigens discovered and was identified by a number of independently developed monoclonal antibodies (mAb) 17-1A, 323/A3, and MOC31 [13]. EpCAM is a 40kD type I transmembrane glycoprotein involved in cell-to-cell interactions and adhesions [14]. The molecule is under physiological conditions minimally expressed on the basolateral surface of epithelial cells and in undifferentiated pluripotent stem cells [15]. However, it is overexpressed in virtually all epithelial cancers and expression is conserved with cancer progression and metastasis [16]. EpCAM is associated with cellular signaling processes and plays a prominent role in tumor cell migration, proliferation and differentiation [17]. Very high overexpression (100–1000 fold) of EpCAM has been found in colorectal, gastric, esophageal, head-and-neck, breast and gynecological cancers with cell surface copy numbers ranging between 100,000 and 300,000 [18–20]. Consequently, EpCAM-targeting therapeutic antibodies were studied in phase I, II and III trials in various cancer types including ovarian-, gastric- and head-and-neck cancer and peritonitis carcinomatosa [21–23].

In this study, we combined two well-known clinically tested components: an antigen binding fragment (Fab) derived from the antibody MOC31 [24] and the fluorophore IRDye800CW® [25,26]. The first iteration of the antibody Fab fragment has already been tested in preclinical and clinical studies as the immunotoxin VB6-845, constructed as a recombinant fusion protein [27]. The fluorophore IRDye800CW has previously been conjugated to cetuximab and bevacizumab, and showed visualization of respectively head-and-neck cancer and breast cancer in early phase clinical trials [9,10].

The aim of this study was to develop and validate a clinical translatable EpCAM-specific NIR fluorescent imaging agent that can be used for visualization of multiple tumor types. Application of EpCAM-F800 during oncological surgeries can potentially aid real-time detection of tumors, assist clinical decision making and improve treatment strategies for cancer patients in the near future.

2. Materials and methods

2.1. Human samples and staining

Paraffin-embedded tissue blocks from 10 patients who underwent surgical resection of rectal cancer between 2014 and 2015 were obtained at the Pathology Department of the Leiden University Medical Center (LUMC) to study the effect of neoadjuvant therapy on EpCAM expression in rectal cancer tissue. Five patients did and five patients did not receive neoadjuvant CRT. Tissue blocks containing tumor tissue and blocks containing adjacent normal rectal tissue were obtained. After sectioning, slides were stained for EpCAM using mAb MOC31 (Millipore Sigma, Saint Louis, MO, USA) in a predetermined optimal dilution of 1:10,000. After overnight incubation, DAKO envision + HRP anti-mouse was added for 30 min (K4001; DAKO Cytomation, Glostrup, Denmark) followed by diaminobenzidine solution (DAB+; DAKO Kit) to visualize EpCAM expression. All sections were counterstained with hematoxylin, dehydrated and finally mounted with pertex. All samples were handled in an anonymous fashion according to the National Ethical Guidelines ('Code for Proper Secondary Use of Human Tissue', Dutch Federation of Medical Scientific Societies) and were approved by the Institutional Ethics Committee of the LUMC.

2.2. Fab production, conjugation and stability

VB5-845d (Viventia, Winnipeg, Canada) is a T-cell epitope depleted Fab version of the anti-EpCAM Fab deBouganin fusion protein, VB6-845. To express VB5-845d in *E. coli* supernatant, a dicistronic unit was created where the heavy and light chains were preceded by a PelB leader sequence. The insert was placed under the control of the arabinose promoter and cloned into a pING plasmid. The resulting VB5-845d/pING plasmid was then transformed into E.coli strain E1.04. After L-arabinose induction, the presence of soluble VB5-845d Fab protein in the supernatant was detected by western blot using a human anti-Kappa antibody coupled to HRP (Sigma, St Louis, MO).

In a 20 L Bioreactor containing 15 L of glycerol minimum media, transformed *E. coli* E104 cells were grown to an OD600 of 50 and induced with L-arabinose. Following induction, the supernatant was collected by centrifugation, clarified by microfiltration, concentrated and diafiltrated prior to loading onto a KappaSelect column (GE Healthcare Life Sciences, Mississauga, Canada). After the column was washed with equilibration buffer, bound VB5-845d was eluted with 0.1 M Glycine-HCl, pH 2.5 and neutralized to pH 7.0 with Tris buffer. The fractions containing VB5-845d were then flowed-through a Q-sepharose column (GE Healthcare Life Sciences, Mississauga, Canada) and the effluent loaded on to an SP-sepharose (GE Healthcare Life Sciences, Mississauga, Canada). Bound VB5-845d was eluted, filter sterilized and frozen at −20 °C. Purity and stability was confirmed by Coomassie staining and SE-HPLC and identity by Western blot analysis. Protein concentration was determined by BCA (Thermo Fisher Scientific, Waltham, MA, USA).

The 800CW NHS-ester (excitation peak at 773 nm, emission peak at 792 nm) and DOTA were both stored according to manufacturer protocol. Anti-EpCAM Fab VB5-845d was covalently conjugated to 800CW (EpCAM-F800) or DOTA (EpCAM-F-DOTA) using N-Hydroxysuccinimide (NHS) ester chemistry against primary amines following manufacturer protocol (Thermo Fisher Scientific, MA, USA) and as briefly described in the supplementary data. For 800CW, Maldi-TOF analyses were performed using a Microflex (Bruker) and sinnapinic acid as matrix to evaluate labelling ratios.

The affinity of anti-EpCAM Fab and EpCAM-F800 to recombinant His-tagged EpCAM (Sino Biological) was determined using a Biacore T200 (GE Life Science). The EpCAM protein was immobilized using the His-tag on the flow cell 2 of the NTA-Chip to the level of ~150 RU. Fabs were injected in five sequential increasing concentration over flow cells 1 and 2 with flow cell 1 used as the binding reference. After each experiment the surface of the chip was regenerated from bound Fab and immobilized EpCAM using SDS and EDTA solutions. The data was fitted according to the 1:1 Binding kinetics model using Biacore T200 evaluation software.

2.3. Human cancer cell lines

After evaluation of a panel of human cancer cell lines for EpCAM expression, four human cancer cell lines were selected; two from colorectal cancer origin (HT-29 and Colo320) and two from breast cancer origin (MCF-7 and MDA-MB-231). The latter was a kind gift from drs J. Gostner and G. Spizzo, (Medical Universität Innsbruck). All cell lines were free of mycoplasma and were cultured in RPMI1640 (PAA) supplemented with 10% fetal bovine serum (Gibco) and 100 I.U./mL penicillin/streptomycin (PAA) in a humidified incubator at 37 °C and 5% CO_2. The HT-29-luc2 cell-line was established and validated by our own research group [28].

2.4. Flowcytometry and fluorescent affinity assays

Identical protocols for flowcytometry and fluorescent affinity assays were used as recently described [28] and are described in detail in the supplementary materials. The number of EpCAM molecules per cell were established using the Qifikit (DAKO) as described before using

anti-EpCAM monoclonal antibodies 323/A3 [29].

2.5. Animal models

The Animal Welfare Committee of the LUMC assessed all animal experiments for animal health, ethics, and research goals and approved the studies. All animals received humane care and maintenance in compliance with the 'Code of Practice Use of Laboratory Animals in Cancer Research'. Similar animal models were used as previously described [30] and are extensively described in the supplementary materials. In short, six-week-old, athymic, female mice were either injected subcutaneously with HT-29-luc2 cells (5.0×10^5 cells per spot) at 4-sides on the back, to induce subcutaneously colorectal tumors, or were inoculated with 2.5×10^5 MCF-7-luc2-cGFP cells in two contralateral mammary fat pads, to induce orthotopic breast tumors. For the colorectal orthotopic model, subcutaneously growing HT-29-luc2 tumors were harvested, cut in small fragments, and transplanted onto the cecal wall.

2.6. NIR fluorescence imaging systems

Imaging was performed using the Pearl® Impulse small animal imager (LI-COR, Lincoln, NE, USA) and the Artemis imaging system (Quest Medical Imaging, the Netherlands). Identical imaging set-ups were used as previously described [30]. Detailed information is provided in the supplementary material section.

2.7. In vivo specificity

The binding specificity of EpCAM-F800 was explored using an *in vivo* blocking experiment. Mice bearing subcutaneous colorectal tumors (HT-29-luc2) received 4 h prior to IV injection of 1 nmol (52 μg) EpCAM-F800 an intra-peritoneal injection of a 10 times higher dose of unlabeled Fab (10 nmol, 520 μg, n = 4). NIR fluorescence images were acquired at 24 and 72 h post-injection with both the Pearl and the Artemis imaging system. After the last measurement, animals were sacrificed. Tumor-to-background ratios (TBRs) were generated by drawing regions of interest (ROIs) on tumors and surrounding tissue, at the back of the mice between the tumors, on fluorescence images. TBRs were calculated by dividing the mean fluorescence signals detected in tumor by the mean signals in the surrounding tissue.

2.8. In vivo binding characteristics, dose finding and biodistribution

When subcutaneous HT-29 colorectal tumors were sized 36 ± 6 mm^2, either 1/16 nmol (3.3 μg), 1/4 nmol (13 μg), 1 nmol (52 μg), 5 nmol (260 μg), 10 nmol (520 μg) or 20 nmol (1040 μg) EpCAM-F800 was intravenously injected (n = 3 per dose group). At 4, 8, 24, 48, 72 and 96 h post injection, fluorescence was measured using the Pearl® and the Artemis imaging system. Biodistribution was studied measuring the fluorescence signal in mice bearing HT-29-luc2 tumors with either EpCAM-mAb800 or EpCAM-F800 or control mice without injection of EpCAM-F800. In total, 6 mice were injected with 1 nmol of EpCAM-mAb800 (150 μg) and sacrificed at 24 (n = 3) or 72 h (n = 3) post injection. The same experiment was performed in mice injected with EpCAM-F800 (52 μg, n = 6) and control mice (n = 6). Biodistribution was calculated by measuring the fluorescence intensity of all excised organs, as well as of blood, urine and feces [29].

2.9. Radiolabeling and biodistribution

Radiolabeling was performed by dissolving EpCAM-F-DOTA in 0.1M HEPES buffer (10 μg/100 μl) and adding indium-111 chloride (35 MBq $^{111}InCl_3$, Covidien-Mallinckrodt, Dublin, Ireland). After 30 min of incubation on the shaker, labelling was validated by HPLC (JASCO, Easton, USA). In all cases, labelling efficacy was > 90%. To study the biodistribution, 6 mice were intravenously injected with 1 nmol (50 μg) ^{111}In-EpCAM-F-DOTA.

. Mice were sacrificed 24 (n = 3) or 72 h (n = 3) post injection and organs were excised, weighted, and measured for radioactivity with a gamma counter (Wizard2 2470 automatic gamma scintillation counter, Perkin Elmer, USA). Activity was divided by the weight of each tissue to calculate the percentage injected dose per gram (%ID/g).

2.10. Pharmacokinetic analysis

Pharmacokinetic analysis was performed as previously described (30). Briefly, EpCAM-F800 was diluted in human whole blood to the concentrations 2.0, 1.0, 0.5, 0.25, 0.13, 0.06, 0.03, 0.02, $7.81*10^{-3}$, $3.90*10^{-3}$, $1.95*10^{-3}$, $9.76*10^{-4}$ μM. A calibration curve was created by measuring each concentration in a 75 μl capillary tube using the Pearl® imaging system. Data was plotted in fluorescence intensity over concentration (μM). Subsequently, four mice were injected with 5 nmol EpCAM-F800 via the lateral tail vein. The contralateral lateral tail vein was used to draw blood 5 min before and 1, 30, 60, 90, 120, 180, 240, 360 and 1440 min post injection. Blood samples were absorbed using 75 μl capillary tubes and immediately measured using the Pearl® imaging system. Each measurement was extrapolated to its concentration using the calibration curve. Data were plotted in logarithmic concentration (μM) over time (min).

2.11. Histology and NIR fluorescence microscopy

Tumor penetration of EpCAM-F800 was assessed in colorectal tumors, obtained from 8 mice bearing subcutaneous HT-29-luc2 tumors. Mice were sacrificed at 1 (n = 2), 4 (n = 2), 8 (n = 2) or 24 h (n = 2) after injection of either 1 or 10 nmol EpCAM-F800. Tumors were snap frozen in isopentane and stored at −80 °C. Tissues were sectioned at 10 μm, stained with DAPI and subsequently fluorescence imaging was performed using a Leica DM5500B digital microscope (Leica Microsystems B.V., Son, the Netherlands). Adjacent slides were hematoxylin-eosin (HE) stained.

Specificity of EpCAM targeted fluorescence in HT-29 tumors after injection of EpCAM-F800 was confirmed by immunohistochemical staining of EpCAM using a 323/A3, an anti-EpCAM mAb targeting a different epitope. HT-29 tumors were resected 24 h post injection of 5 nmol EpCAM-F800 and snapfrozen in isopentane. Subsequently, fluorescence imaging of 5 μm tissue sections on slides was performed using the Odyssey imager (LI-COR, Lincoln, NE, USA) at 800 nm after which they were HE-stained. Adjacent slides were used for fluorescence microscopy and immunohistochemistry. To confirm the presence of EpCAM, slides were stained using 323/A3-Alexa488 by fixation in acetone for 10 min and incubation with 5 μg/ml of the antibody, followed by washing. Slides stained for EpCAM, and unstained slides, were mounted with Prolong Gold with DAPI and analyzed with a Leica DM5500B digital microscope using L5 and Y7 filter cubes for detecting Alexa488 and 800CW respectively.

2.12. Calculations and statistical analyses

Statistical analysis and generation of graphs were performed using GraphPad Prism software (version 5.01, GraphPad Software Inc, La Jolla, CA, USA). Differences between groups in the *in vitro* binding assays were analyzed using the Mann-Whitney *U* test. Tumor-to-background ratios (TBR) were calculated by drawing regions of interest (ROIs) on fluorescence images from the Pearl® small animal imager or Artemis imaging system to extract mean signal for tumors and all major organs. Organ-to-blood ratios were calculated by dividing each value by the mean fluorescence signal detected in the tissue and blood and reported as mean and standard deviation. The two-way repeated measurement ANOVA, used to assess the relation between TBRs in different dose groups and time points, was corrected for multiple comparisons

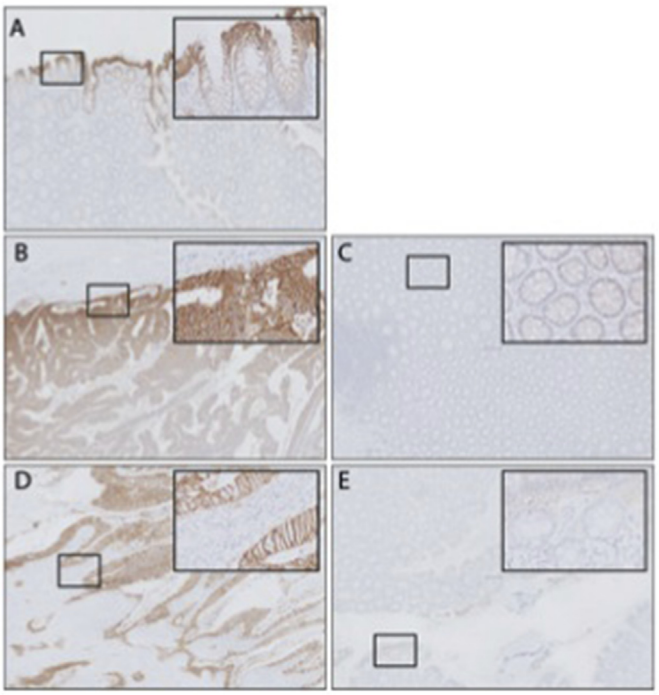

Fig. 1. A) Example of EpCAM expression on normal rectal tissue; EpCAM expression is confined to the luminal side of the epithelium. **B)** Example of EpCAM expression on a distal rectal cancer of a patient who was not treated with neoadjuvant therapy. **C)** EpCAM expression on the corresponding normal rectal tissue of the same patient. **D)** EpCAM expression on a proximal rectal cancer of a patient who has been treated with neoadjuvant therapy. **E)** EpCAM expression on the corresponding normal rectal tissue of the same patient. (5x and 40x enlargements).

using the Bonferroni correction.

3. Results

3.1. EpCAM expression on human rectal (cancer) tissues and cell lines

Normal rectal tissue showed weak/moderate expression of EpCAM, which was mostly limited to enterocytes located at the tip of the villi (Fig. 1A). All rectal cancer tissues showed an intense, homogeneous EpCAM expression with a circumferential staining pattern (Fig. 1B and D). EpCAM expression on tumor tissue and adjacent normal epithelium did not differ between tissues derived from patients who were not (Fig. 1B and C) and who were (Fig. 1D and E) treated with neoadjuvant CRT.

The selection of cell lines for the *in vivo* studies was based on flow cytometry of panels of breast and colon cancer cell lines (for the latter see Suppl. Fig. S0). Cell lines MCF-7 and HT-29, both with intermediate EpCAM expression, were selected. The number of EpCAM molecules per cell, as determined using 2 different monoclonal antibodies in combination with Qifikit, confirmed the data obtained by plain flow cytometry. The positive colon cancer cell line HT-29 expressed 195,000–197,000 copies (323/A3 versus MOC31) and the breast cancer cell line MCF-7 255,000–265,000 copies. The control cell lines Colo320 and MDA-MB-231 showed numbers under the detection limit of the assay (< 1000).

3.2. Fab conjugation, binding capacity and stability

Little to no expression of EpCAM was seen on the control Colo-320 and MDA-MB-231 cell lines using Fab VB5-845d and positive control MOC31, while high expression of EpCAM was measured on HT-29 and

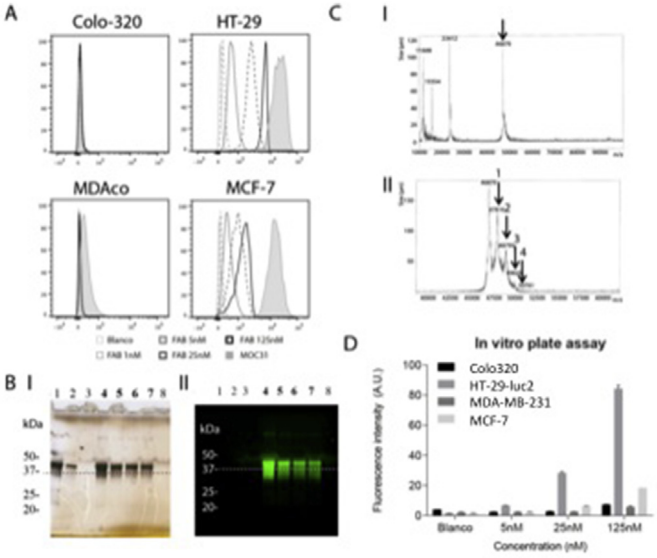

Fig. 2. A) Binding capacity of Fab for EpCAM using flow-cytometry. As positive control, the anti-human EpCAM monoclonal antibody MOC31 was used confirming the high and low expression levels of EpCAM on the tumor cells. Enhancing the concentration of Fab resulted in an increase in signal on the cells with high EpCAM expression. **B)** Conjugation was evaluated using SDS-PAGE gel (4–20%). Unconjugated Fab in lane 1 (10 μg) and lane 2 (1 μg) and EpCAM-F800 in lane 4 (10 μg), lane 5 (5 μg), lane 6 (5 μg) and lane 7 (5 μg) while lane 3 and lane 8 are empty. EpCAM-F800 was clearly visible at approximately 45 kDa both with silver staining and fluorescence. **C)** I, Maldi-TOF analysis of Fab showed one clear peak at 46870 Da with a purity of > 98%. II, extra peaks appeared at 47816Da (1), 48795Da (2), 49820Da (3) and 50761Da (4) representing respectively 1, 2, 3 and 4 IRDye800CW labels per Fab. **D)** Plate assay analysis showed retained binding capacity of EpCAM-F800 on all four cell lines after conjugation. Increasing the concentration increased the fluorescent intensity for the high expressing cell lines.

MCF-7 cell lines (Fig. 2A). Conjugation was evaluated using SDS-PAGE showing EpCAM-F800 at approximately 45 kDa by silver staining (Fig. 2B I) and by NIR fluorescence imaging (Fig. 2B II). No degradation products were seen. Before conjugation, the Fab showed > 98% purity (Fig. 2C I) and after conjugation, Maldi-TOF analysis indicated that the majority of Fab molecules were conjugated with an average of 1–4 dye molecules (Fig. 2C II). Higher concentrations of EpCAM-F800 resulted in higher signals on the EpCAM expressing cell lines, while almost no signal was measured in the low expressing control cell lines (Fig. 2D). The calculated K_D of anti-EpCAM Fab was with 90 pM comparable to those of MOC31 and 323/A. Although conjugation with the fluorescent dye 800CW diminished the affinity approximately 25 times, this is still considered high affinity.

3.3. In vivo biodistribution

At 24 h post injection, the liver, kidneys and urine showed higher fluorescence signals than the tumor (Fig. 3A). Compared to EpCAM-F800, injection of EpCAM-mAb800 resulted both at 24 and 72 h in a significantly higher signal in the liver (Fig. 3A and B). Due to the smaller size of EpCAM-F800 and renal clearance, fluorescence in the kidneys was higher after 24 h than EpCAM-mAb800. In contrast, 72 h after injection of EpCAM-mAb800 all measured organs showed higher signal intensity compared to EpCAM-F800 (Fig. 3B). At 24 h and 72 h post injection of EpCAM-mAb800, the intensity of fluorescence in blood was respectively 3 and 6 times higher than the fluorescence measured after injection of EpCAM-F800. Biodistribution of all organs after injection of EpCAM-mAb800, EpCAM-F800 and of control mice, without injection of any dye, are shown in Figs. S1 and S2. TBRs were significantly higher for EpCAM-F800 compared to its full size variant

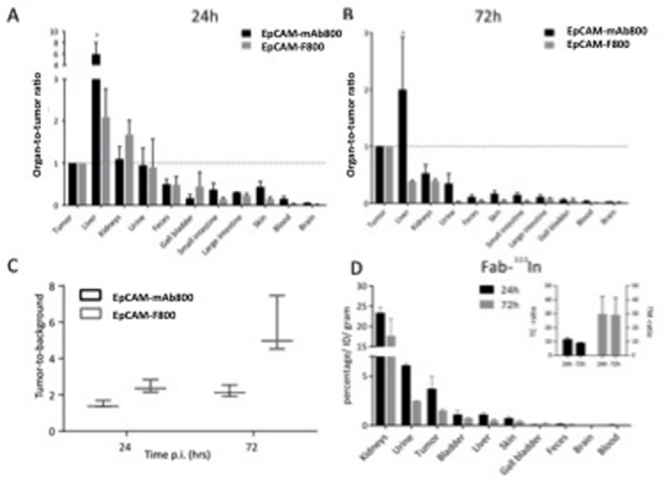

Fig. 3. A) Biodistribution of EpCAM-mAb800 and EpCAM-F800 presented as organ-to-tumor ratio at 24 h post injection of 1 nmol. High fluorescence was seen in metabolizing organs and in the urine. Intensity of the fluorescence signal in the liver was significantly higher after injection of EpCAM-mAb800 compared to EpCAM-F800. Higher fluorescence signals in the kidneys after injection of EpCAM-F800 are most probably the result of renal clearance of the Fab fragment. (* = $p < 0.05$) **B)** Biodistribution of EpCAM-mAb800 and EpCAM-F800 presented as organ-to-tumor ratio at 72 h post injection of 1 nmol. All organs showed higher fluorescence signals after injection of EpCAM-mAb800 compared to EpCAM-F800. Fluorescence in the liver was significantly higher compared to EpCAM-F800. **C)** Significant higher TBRs were measured for EpCAM-F800 both at 24 h and 72 h post injection compared to EpCAM-mAb800. The fluorescence signal measured at the back of the mice, between tumors, was considered as background signal. **D)** Biodistribution of ^{111}In-EpCAM-F-DOTA shown as %/ID/gram at 24 h and 72 h post injection.

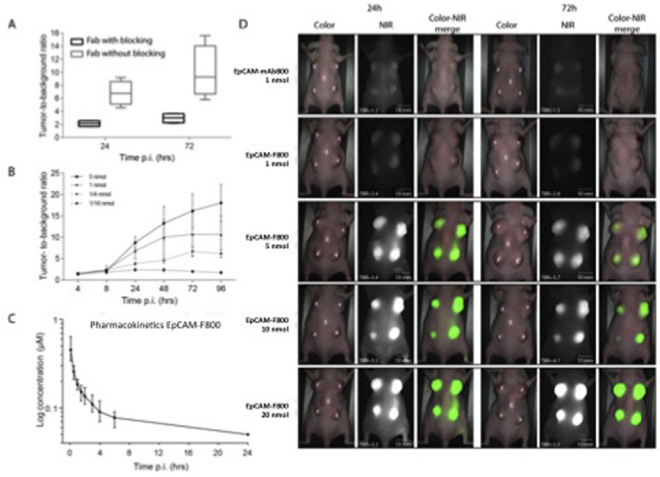

Fig. 4. A) Blocking with unlabeled Fab fragments significantly ($p < 0.05$) decreased the tumor-to-background ratios at both the 24 h (6.81 ± 1.65 vs. 2.34 ± 0.42) and 72 h (10.01 ± 3.544 vs. 2.96 ± 0.638) time-point. **B)** Tumor-to-background ratios (TBR) are shown over time for the 1/16 to 5 nmol dose groups. **C)** Pharmacokinetic results, displayed in a logarithmic scale. A mean blood half-life time of 4.5 h was measured. **D)** Examples of *in vivo* images of mice bearing subcutaneous tumors acquired at 24 and 72 h post injection with EpCAM-mAb800 or different doses of EpCAM-F800. The white regions of interest are used as background to calculate TBRs. All images are normalized and acquired with the Artemis imaging system. (# tumors of different sizes).

EpCAM-mAb800 at both 24 h and 72 h post-injection (Fig. 3C).

Quantitative measurements of the biodistribution were performed using ^{111}In-EpCAM-F-DOTA (1 nmol). The total mean activities for the mice sacrificed at 24 h post injection were 5.7 ± 0.1%ID/g and at 72 h were 5.2 ± 0.3%ID/g (MBq, mean ± SD). The biodistribution study confirmed accumulation of ^{111}In-EpCAM-F-DOTA in subcutaneous colorectal tumors and the kidneys at 24 h, with significant lower values at the 72 h time-point (selection in Fig. 3D and full in Fig. S3). Compared to the signal intensity from the intestine, relatively high intensity signals were observed in the skin, thereby influencing TBRs, as also seen with NIR fluorescence in this subcutaneous model. Mean tumor-to-colon (TC) ratio was 11.5 ± 1.5 at 24 h and 8.9 ± 0.7 at 72 h and mean tumor-to-muscle (TM) ratio was 29.6 ± 12.8 at 24 h and 29.0 ± 12.5 at 72 h.

3.4. In vivo blocking and dose optimization study

Tumor binding of EpCAM-F800 was further validated using a blocking experiment by competing with the unlabeled Fab fragment. The group with a pre-injection of unlabeled Fab showed significant lower TBRs at 24 h post injection compared to the group without the pre-injection (2.1 ± 0.4 vs. 6.8 ± 1.7, $p < 0.05$) and the difference increased further at 72 h (3.0 ± 0.6 vs. 10.0 ± 3.5, $p < 0.05$) (Fig. 4A).

Dose optimization studies showed increasing TBRs for all doses at 4 h post injection (Fig. 4B & S4). For the 24 h time-point, a significant difference was observed between 1 nmol versus 1/16 nmol ($p < 0.05$) and no significant differences were seen between 1 nmol and higher doses, possibly due to saturation of the receptors (Fig. 4B). For the 48 h time-point, TBRs measured with 1 nmol only differed significant from 1/16 ($p < 0.05$) and 1/4 nmol ($p < 0.05$). Absolute signals in both tumor and background decreased significantly within the first 4 h after injection of 1 and 5 nmol (Fig. S4). The maximal concentration of EpCAM-F800 in blood measured at 1 min post injection was 59 µM (Fig. 4C). Decrease of EpCAM-F800 blood concentrations followed a biphasic pattern with a distribution and elimination phase with a mean terminal half-life of 4.5 h, and with an area under the curve (AUC) of approximately 63 µg*h/mL. Mean systemic clearance was 0.08 ± 0.03 mL/min. Fig. 4D shows examples of images captured with the intraoperative Artemis imaging system. Increasing the dose over 5 nmol resulted in higher fluorescence signals in both tumors and background, but not in higher TBRs (Fig. S5).

3.5. Clinical relevant orthotopic models

In the orthotopic breast cancer (MCF-7) model TBRs increased significantly up to 48 h (Fig. 5A) after injection of 1 nmol EpCAM-F800. Due to the relatively short blood half-life, absolute signals in the background decreased faster than signals in the tumor. Fig. 5B shows an example of *in vivo* breast tumor detection using the Artemis imaging system. Tumors could be recognized at 24 h and 72 h post injection and images from all time points are shown in Fig. S6. In the colorectal tumor model, mean TBRs increased significantly between 24 h and 72 h time-points (4.2 ± 0.2 at 24 h vs. 6.6 ± 0.8 at 72 h, $p < 0.05$) after injection of 1 nmol of EpCAM-F800 (Fig. 5C). Similar to the breast cancer model, absolute signals in the background decreased faster than the signals in the tumors between 24 h and 72 h (46% versus 72%). Fig. 5D shows an example of images captured by the Artemis imaging system and bioluminescence (BLI), confirming the presence of tumor tissue. Moreover, millimeter-sized fluorescent nodules could be visualized and confirmed by BLI.

3.6. Histology and NIR fluorescence microscopy

Fluorescence microscopy revealed a clear difference in penetration pattern and intensity after 1 and 4 h post injection (Fig. 6A). After 1 h fluorescence was mainly present in a rim around the tumor cells. After 4 h, fluorescence was seen throughout the whole tumor indicating full penetration of EpCAM-F800 in tumors between 1 and 4 h after injection. Moreover, the level of fluorescence intensity retained in tumors

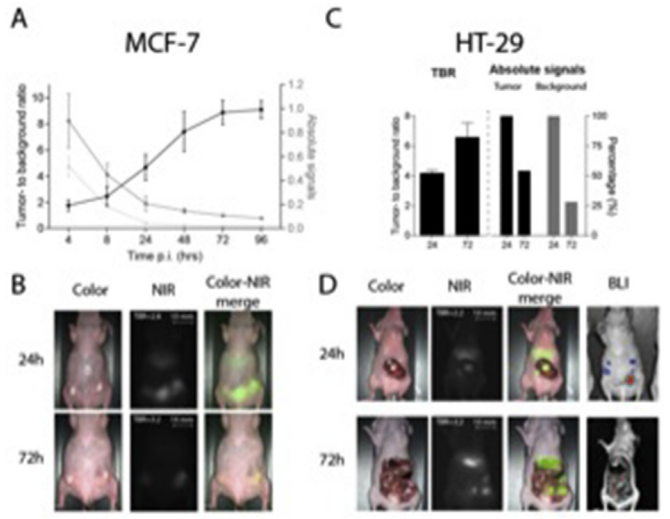

Fig. 5. A) Tumor-to-background ratios and absolute signals of EpCAM-F800 in the orthotopic MCF-7 model over time. **B)** Examples of images acquired with the Artemis imaging system at 24 and 72 h. In white, the background regions are shown used to calculate TBRs. **C)** TBRs at 24 and 72 h and mean absolute signals at these time-points of 0.51 ± 0.08 and 0.12 ± 0.02 at 24 h post injection (shown as 100%) for respectively the tumor and the background, and 0.28 ± 0.07 and 0.04 ± 0.01 at the 72 h time point are shown. **D)** Examples of images taken with the Artemis imaging system and BLI showing the co-localization of the fluorescent lesions with the colorectal tumors (Organs were slightly altered between fluorescent and BLI measurements. The background regions used to calculate TBRs are indicated by white stars (# tumors of different sizes).

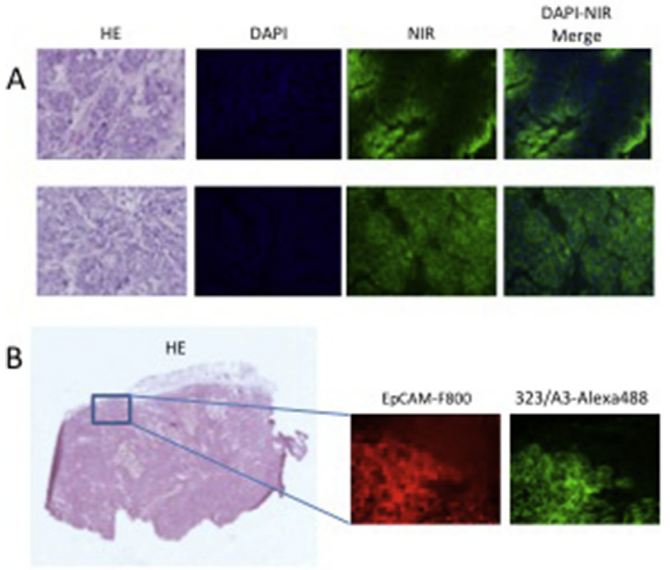

Fig. 6. A) Fluorescence histology of HT29-tumors, obtained 1 and 4 h after injection of 10 nmol EpCAM-F800. Shown are respectively HE staining, DAPI staining, fluorescence microscopy images and overlay images (DAPI and fluorescence) of representative tumor slices 1 and 4 h after injection of EpCAM-F800. After 1 h, tumor penetration of EpCAM-F800 is limited to the tumor borders, while fluorescence is seen throughout the complete tumor after 4 h. **B)** Fluorescence histology of a HT-29 tumor, harvested from a mouse injected with 5 nmol EpCAM-F800, shows co-localization of EpCAM-F800 and 323/A3-Alexa488.

between 4 and 24 h, possibly due to internalization of the agent. NIR fluorescence microscopy images of colorectal tumors revealed co-localization of EpCAM-F800 and 323/A3-Alexa488, indicating that EpCAM-F800 targets EpCAM (Fig. 6B).

4. Discussion

This study investigates an anti-EpCAM Fab fluorescent agent that can demarcate multiple tumor types *in vivo* using real-time fluorescence imaging. Due to the generally high overexpression on carcinomas, EpCAM is considered as one of the most promising generic tumor targets which is also recognized by the National Cancer Institute [23,31]. Highest expression patterns are found in colorectal cancers as well as their metastasis [19]. The reported levels of EpCAM overexpression around 200,000–300,000 copies per cell are confirmed for the positive cell lines used in this study, reaching the low-end range of the gene-amplification based tumor marker HER2/Neu (200,000 to 10 million copies per cell).We show that EpCAM overexpression is preserved in rectal cancer tissue after neoadjuvant therapy, a crucial characteristic for a potential candidate oncotarget. Various EpCAM specific antibodies are clinically tested for their therapeutic effect, with dosages far above the dose suggested for tumor imaging. Unfortunately, little or no overall survival benefit was shown and affinity related side effects were observed hampering their clinical utility [32]. However, this does not make EpCAM a useless target for imaging purposes. After all, imaging tracers require a much lower dose compared to therapeutic agents, which usually avoids potential side effects.

EpCAM has been evaluated as a target for imaging applications utilizing antibodies, antibody fragments and aptamers conjugated to fluorescent dyes, radionuclides or both [33–35]. Zhu et al. described the use of an EpCAM-specific NIR fluorescent imaging agent for the recognition of tumor margins in a human prostate cancer orthotopic mouse model and showed accurate detection of both primary and metastatic lesions [35]. We recently conjugated the monoclonal antibody 323/A3 to IRDye800CW and showed clear tumor demarcation in breast, head-and-neck and colorectal cancer xenograft models at 72 h post injection [34]. Although antibodies are believed to possess superior binding characteristics compared to smaller molecules [36,37], their relatively large size (~150 kDa) might result in heterogeneous tumor distribution, complex pharmacokinetics, and long imaging lead-times (up to 72 h) as shown in this and our previous study [30]. On the other hand, Fab fragments are three times smaller and show more homogenous tumor penetration. Moreover, they display shorter half-life times, a decreased immunotoxicity potential [38,39] while they are large enough to maintain high plasma levels for optimal (tumor) distribution [40–43]. Although smaller vehicles like nanobodies or peptides may result in even better pharmacokinetic properties (e.g. faster clearance), they can have lower stability and affinity (for example, linear peptides vs. scFv fragments), and are more compromised by conjugation compared with antibodies or antibody fragments. EpCAM-F800 is being produced for clinical use and experiments were therefore performed with a clinically validated imaging system and an already clinically tested NIR fluorescent dye, in order to expedite clinical translation. The anti-EpCAM antibody fragment we specifically developed is a Fab fragment of its full antibody variant, 4D5 MOC-B [44]. It is deimmunized, to tackle potential immunogenicity. A non-deimmunized variant was already used in a first-in-human clinical trial, where it was fused with a deimmunized variant of the plant-derived toxin bouganin [27]. Deimmunization is important because it lowers the chance of an immune response. Hence, it allows repeated use in patients undergoing multiple surgeries or participating in tumor screening programs. Conjugation with the dye was performed using the generally accepted NHS-method, with conditions leading to stable dye/protein-labelling ratios of around 1.5. Preclinical studies showed that IRDye800CW is not immunogenic with a no adverse effect level (NOAEL) of 20 mg/kg [25]. The advantage of IRDye800CW with respect to other NIR fluorescent dyes is its water-solubility in combination with high signal intensity. Water-solubility enables conjugation in water-based solutions, which simplifies the purification process substantially and

simplifies production under current Good Manufacturing Practices (cGMP) conditions.

The limited effect of the enhanced permeability and retention (EPR) effect was shown in the *in vivo* blocking experiment, where a 3–4 times lower TBR was measured after pre-injection with the unlabeled agent. The stagnating TBRs in the higher dose groups (5–20 nmol) clearly show the concentration at which saturation of available EpCAM binding places occurred. The optimal dose range of EpCAM-F800 for fluorescence tumor detection, i.e. 1–5 nmol in mice (52–260 μg), corresponds with a dose of 0.16–0.8 mg/kg in humans, adjusted for body surface area [45].

Biodistribution showed a classical Fab distribution pattern with high TBRs and high signals in the tumor and excreting organs. Due to the glomerular-filtration cut-off of 60 kDa, most of the agent is excreted via the kidneys. The observed high fluorescence signals in the liver may be explained by the lipophilicity and negative charge of IRDye800CW, which leads to increased albumin binding and adjacent liver accumulation. This is underscored by the fact that no significant liver uptake could be measured with ^{111}In-EpCAM-F-DOTA [46]. One should bear in mind that certain factors influence fluorescence intensity during biodistribution studies, such as absorbance of photons by adjacent tissue and scattering properties.

The half-life time of EpCAM-F800 in mice was estimated at 4.5 h, which is in concordance with VB6-845 in humans [27]. Although the total circulation time of EpCAM-F800 is relatively short (10–20 h), it is sufficient to allow adequate tumor penetration; homogenous signals throughout the tumor were seen at 4 h post injection.

Two clinically relevant orthotopic mouse models were investigated using the Artemis imaging system. In this set-up real-time tumor-specific visualization of colorectal and breast tumors was shown with high TBRs between 8 and 24 h. Besides these tumor types, application of EpCAM-F800 may aid detection of multiple other epithelial-derived cancers due to overexpression of EpCAM. Prior to the clinical introduction of EpCAM-F800, toxicology studies need to be performed. Our preliminary data of a generic single extended dose toxicology study in rats show no test item-related mortality, clinical signs and effects on body weight, food consumption, clinical pathology and organ weight after injection of approximately 50 and 100 times the intended human dose of EpCAM-F800. Following the promising preclinical and toxicology results, EpCAM-F800 first-in-human studies can be designed as first step towards clinical translation. After successful first-in-human studies, a possible additional study design might be to detect tumor growth during fluorescence endoscopy in patients previously treated with neoadjuvant CRT. Suitable patients can be straightforward selected preoperatively with immunohistochemistry on biopsy specimens using either MOC31 or the Fab fragment.

In conclusion, we demonstrate the successful development, evaluation and feasibility of EpCAM-F800 for intra-operative tumor detection using fluorescence imaging. Although only breast and colorectal tumor models were described, application of EpCAM-F800 is expected to provide surgeons with a highly sensitive imaging tool to improve intraoperative visualization of multiple tumor types. Wide implementation of tumor-specific (NIR) fluorescence imaging has the potential to make surgery safer and more precise.

Acknowledgments

We thank Shadhvi Bhairosingh for her contribution with histological procedures.

Appendix A. Supplementary data

Supplementary data to this article can be found online at https://doi.org/10.1016/j.suronc.2018.10.004.

Financial support

This work was supported by the Dutch Cancer Society (grant UL2010-4732, UL2015-8089) and by the European Research Council through an ERC Advanced Grant: project SURVive (grant 323105).

Conflicts of interest

Arjune Premsukh and Jeannick Cizeau are employees of Viventia Bio Inc. and Glen MacDonald is an officer of Eleven Biotherapeutics, both of which have direct financial interest in the subject matter discussed in this manuscript.

References

[1] E. Mois, F. Graur, N.A. Hajjar, et al., The influence of circumferential resection margins on survival following rectal cancer surgery, Ann. Ital. Chir. 88 (2017).
[2] P. Swindle, J.A. Eastham, M. Ohori, et al., Do margins matter? The prognostic significance of positive surgical margins in radical prostatectomy specimens, J. Urol. 179 (2008) S47–S51.
[3] R. Haque, R. Contreras, M.P. McNicoll, et al., Surgical margins and survival after head and neck cancer surgery, BMC Ear Nose Throat Disord. 6 (2006) 2.
[4] S.E. Singletary, Surgical margins in patients with early-stage breast cancer treated with breast conservation therapy, Am. J. Surg. 184 (2002) 383–393.
[5] C.J. van de Velde, P.G. Boelens, J.M. Borras, et al., EURECCA colorectal: multidisciplinary management: European consensus conference colon & rectum, Eur. J. Canc. 50 (2014) 1e1–1e34.
[6] A.L. Vahrmeijer, M. Hutteman, J.R. van der Vorst, et al., Image-guided cancer surgery using near-infrared fluorescence, Nat. Rev. Clin. Oncol. 10 (2013) 507–518.
[7] G.M. van Dam, G. Themelis, L.M. Crane, et al., Intraoperative tumor-specific fluorescence imaging in ovarian cancer by folate receptor-alpha targeting: first in-human results, Nat. Med. 17 (2011) 1315–1319.
[8] C.E. Hoogstins, Q.R. Tummers, K.N. Gaarenstroom, et al., A novel tumor-specific agent for intraoperative near-infrared fluorescence imaging: a translational study in healthy volunteers and patients with ovarian cancer, Clin. Canc. Res. 22 (2016) 2929–2938.
[9] L.E. Lamberts, M. Koch, J.S. de Jong, et al., Tumor-specific uptake of fluorescent bevacizumab-IRDye800CW microdosing in patients with primary breast cancer: a phase I feasibility study, Clin. Canc. Res. 23 (2017) 2730–2741.
[10] E.L. Rosenthal, J.M. Warram, E. de Boer, et al., Safety and tumor specificity of cetuximab-IRDye800 for surgical navigation in head and neck cancer, Clin. Canc. Res. 21 (2015) 3658–3666.
[11] L.S.F. Boogerd, C.E.S. Hoogstins, D.P. Schaap, et al., Safety and effectiveness of SGM-101, a fluorescent antibody targeting carcinoembryonic antigen, for intraoperative detection of colorectal cancer: a dose-escalation pilot study, Lancet Gastroenterol Hepatol 3 (3) (2018 Mar) 181–191, https://doi.org/10.1016/S2468-1253(17)30395-3 Epub 2018 Jan 30.
[12] M. van Oosten, L.M. Crane, J. Bart, et al., Selecting potential targetable biomarkers for imaging purposes in colorectal cancer using TArget selection criteria (TASC): a novel target identification tool, Transl Oncol 4 (2011) 71–82.
[13] M. Herlyn, Z. Steplewski, D. Herlyn, H. Koprowski, Colorectal carcinoma-specific antigen: detection by means of monoclonal antibodies, Proc. Natl. Acad. Sci. U. S. A 76 (1979) 1438–1442.
[14] C. Patriarca, R.M. Macchi, A.K. Marschner, H. Mellstedt, Epithelial cell adhesion molecule expression (CD326) in cancer: a short review, Cancer Treat Rev. 38 (2012) 68–75.
[15] M. Balzar, M.J. Winter, C.J. de Boer, S.V. Litvinov, The biology of the 17-1A antigen (Ep-CAM), J. Mol. Med. (Berl.) 77 (1999) 699–712.
[16] M.J. Winter, I.D. Nagtegaal, J.H. van Krieken, S.V. Litvinov, The epithelial cell adhesion molecule (Ep-CAM) as a morphoregulatory molecule is a tool in surgical pathology, Am. J. Pathol. 163 (2003) 2139–2148.
[17] M. Trzpis, P.M. McLaughlin, L.M. de Leij, M.C. Harmsen, Epithelial cell adhesion molecule: more than a carcinoma marker and adhesion molecule, Am. J. Pathol. 171 (2007) 386–395.
[18] P. Went, M. Vasei, L. Bubendorf, et al., Frequent high-level expression of the immunotherapeutic target Ep-CAM in colon, stomach, prostate and lung cancers, Br. J. Canc. 94 (2006) 128–135.
[19] G. Spizzo, D. Fong, M. Wurm, et al., EpCAM expression in primary tumour tissues and metastases: an immunohistochemical analysis, J. Clin. Pathol. 64 (2011) 415–420.
[20] W.A. Osta, Y. Chen, K. Mikhitarian, et al., EpCAM is overexpressed in breast cancer and is a potential target for breast cancer gene therapy, Cancer Res. 64 (2004) 5818–5824.
[21] G. Riethmuller, E. Schneider-Gadicke, G. Schlimok, et al., Randomised trial of monoclonal antibody for adjuvant therapy of resected Dukes' C colorectal carcinoma. German Cancer Aid 17-1A Study Group, Lancet 343 (1994) 1177–1183.
[22] D. Seimetz, H. Lindhofer, C. Bokemeyer, Development and approval of the trifunctional antibody catumaxomab (anti-EpCAM x anti-CD3) as a targeted cancer immunotherapy, Cancer Treat Rev. 36 (2010) 458–467.
[23] O. Gires, P.A. Bauerle, EpCAM as a target in cancer therapy, J. Clin. Oncol. 28 (2010) e239–240 author reply e241-232.

[24] G.C. MacDonald, M. Rasamoelisolo, J. Entwistle, et al., A phase I clinical study of VB4-845: weekly intratumoral administration of an anti-EpCAM recombinant fusion protein in patients with squamous cell carcinoma of the head and neck, Drug Des. Dev. Ther. 2 (2009) 105–114.
[25] M.V. Marshall, D. Draney, E.M. Sevick-Muraca, D.M. Olive, Single-dose intravenous toxicity study of IRDye 800CW in Sprague-Dawley rats, Mol. Imag. Biol. 12 (2010) 583–594.
[26] K.R. Zinn, M. Korb, S. Samuel, et al., IND-directed safety and biodistribution study of intravenously injected cetuximab-IRDye800 in cynomolgus macaques, Mol. Imag. Biol. 17 (2015) 49–57.
[27] J. Entwistle, J.G. Brown, S. Chooniedass, et al., Preclinical evaluation of VB6-845: an anti-EpCAM immunotoxin with reduced immunogenic potential, Cancer Biother. Radiopharm. 27 (2012) 582–592.
[28] M.C. Boonstra, B. Tolner, B.E. Schaafsma, et al., Pre-clinical evaluation of a novel CEA-targeting near-infrared fluorescent tracer delineating colorectal and pancreatic tumors, Int. J. Canc. 137 (8) (2015 Oct) 1910–1920, https://doi.org/10.1002/ijc.29571 Epub 2015 Jun 22.
[29] H.J.M. Handgraaf, M.C. Boonstra, H. Prevoo, et al., Real-time near-infrared fluorescence imaging using cRGD-ZW800-1 for intraoperative visualization of multiple cancer types, Oncotarget 8 (2017) 21054–21066.
[30] M.C. Boonstra, P.B. Van Driel, D.M. van Willigen, et al., uPAR-targeted multimodal tracer for pre- and intraoperative imaging in cancer surgery, Oncotarget 6 (16) (2015 Jun 10) 14260–14273.
[31] M.A. Cheever, J.P. Allison, A.S. Ferris, et al., The prioritization of cancer antigens: a national cancer institute pilot project for the acceleration of translational research, Clin. Canc. Res. 15 (2009) 5323–5337.
[32] M. Munz, A. Murr, M. Kvesic, et al., Side-by-side analysis of five clinically tested anti-EpCAM monoclonal antibodies, Cancer Cell Int. 10 (2010) 44.
[33] W.E. Meijs, H.J. Haisma, R.P. Klok, et al., Zirconium-labeled monoclonal antibodies and their distribution in tumor-bearing nude mice, J. Nucl. Med. 38 (1997) 112–118.
[34] P.B. van Driel, M.C. Boonstra, H.A. Prevoo, et al., EpCAM as multi-tumour target for near-infrared fluorescence guided surgery, BMC Canc. 16 (2016) 884.
[35] B. Zhu, G. Wu, H. Robinson, et al., Tumor margin detection using quantitative NIRF molecular imaging targeting EpCAM validated by far red gene reporter iRFP, Mol. Imag. Biol. 15 (2013) 560–568.
[36] K.D. Wittrup, G.M. Thurber, M.M. Schmidt, J.J. Rhoden, Practical theoretic guidance for the design of tumor-targeting agents, Methods Enzymol. 503 (2012) 255–268.
[37] A.C. Freise, A.M. Wu, In vivo imaging with antibodies and engineered fragments, Mol. Immunol. 67 (2 Pt A) (2015 Oct) 142–152, https://doi.org/10.1016/j.molimm.2015.04.001 Epub 2015 Apr 28.
[38] S. Gratz, P. Reize, B. Kemke, et al., Targeting of osteomyelitis with IgG and Fab' monoclonal antibodies labeled with [99mTc]: kinetic evaluations, Q. J. Nucl. Med. Mol. Imaging 60 (4) (2016 Dec) 413–423 Epub 2014 Oct 17.
[39] N. Kosaka, M. Ogawa, D.S. Paik, et al., Semiquantitative assessment of the microdistribution of fluorescence-labeled monoclonal antibody in small peritoneal disseminations of ovarian cancer, Cancer Sci. 101 (2010) 820–825.
[40] K.Y. Pak, M.A. Nedelman, W.E. Fogler, et al., Evaluation of the 323/A3 monoclonal antibody and the use of technetium-99m-labeled 323/A3 Fab' for the detection of pan adenocarcinoma, Int. J. Rad. Appl. Instrum. B 18 (1991) 483–497.
[41] R. Watanabe, H. Hanaoka, K. Sato, et al., Photoimmunotherapy targeting prostate-specific membrane antigen: are antibody fragments as effective as antibodies? J. Nucl. Med. 56 (2015) 140–144.
[42] C.T. Mendler, L. Friedrich, I. Laitinen, et al., High contrast tumor imaging with radio-labeled antibody Fab fragments tailored for optimized pharmacokinetics via PASylation, mAbs 7 (2015) 96–109.
[43] D. Li, S. Liu, R. Liu, et al., EphB4-targeted imaging with antibody h131, h131-F(ab') 2 and h131-Fab, Mol. Pharm. 10 (2013) 4527–4533.
[44] J. Willuda, A. Honegger, R. Waibel, et al., High thermal stability is essential for tumor targeting of antibody fragments: engineering of a humanized anti-epithelial glycoprotein-2 (epithelial cell adhesion molecule) single-chain Fv fragment, Cancer Res. 59 (1999) 5758–5767.
[45] S. Reagan-Shaw, M. Nihal, N. Ahmad, Dose translation from animal to human studies revisited, Faseb. J. 22 (2008) 659–661.
[46] K. Valko, S. Nunhuck, C. Bevan, et al., Fast gradient HPLC method to determine compounds binding to human serum albumin. Relationships with octanol/water and immobilized artificial membrane lipophilicity, J. Pharmacol. Sci. 92 (2003) 2236–2248.